Biochimica et Biophysica Acta 1828 (2013) 327–339

Contents lists available at SciVerse ScienceDirect

Biochimica et Biophysica Acta

journal homepage: www.elsevier.com/locate/bbamem

How the amyloid-β peptide and membranes affect each other: An extensive simulation study

Chetan Poojari [a], Andreas Kukol [b], Birgit Strodel [a,c,*]

[a] Research Centre Jülich, Institute of Complex Systems: Structural Biochemistry, 52425 Jülich, Germany
[b] University of Hertfordshire, School of Life Sciences, College Lane, Hatfield AL10 9AB, United Kingdom
[c] Institute of Theoretical and Computational Chemistry, Heinrich Heine University Düsseldorf, 40225 Düsseldorf, Germany

ARTICLE INFO

Article history:
Received 26 March 2012
Received in revised form 3 September 2012
Accepted 4 September 2012
Available online 10 September 2012

Keywords:
Amyloid-beta peptide
Phospholipid membranes
Molecular simulations
Water permeation
Alzheimer's disease

ABSTRACT

The etiology of Alzheimer's disease is thought to be linked to interactions between amyloid-β (Aβ) and neural cell membranes, causing membrane disruption and increased ion conductance. The effects of Aβ on lipid behavior have been characterized experimentally, but structural and causal details are lacking. We used atomistic molecular dynamics simulations totaling over 6 μs in simulation time to investigate the behavior of $A\beta_{42}$ in zwitterionic and anionic lipid bilayers. We simulated transmembrane β-sheets (monomer and tetramer) resulting from a global optimization study and a helical structure obtained from an NMR study. In all simulations $A\beta_{42}$ remained embedded in the bilayer. It was found that the surface charge and the lipid tail type are determinants for transmembrane stability of $A\beta_{42}$ with zwitterionic surfaces and unsaturated lipids promoting stability. From the considered structures, the β-sheet tetramer is most stable as a result of interpeptide interactions. We performed an in-depth analysis of the translocation of water in the $A\beta_{42}$-bilayer systems. We observed that this process is generally fast (within a few nanoseconds) yet generally slower than in the peptide-free bilayers. It is mainly governed by the lipid type, simulation temperature and $A\beta_{42}$ conformation. The rate limiting step is the permeation through the hydrophobic core, where interactions between $A\beta_{42}$ and permeating H_2O molecules slow the translocation process. The β-sheet tetramer allows more water molecules to pass through the bilayer compared to monomeric Aβ, allowing us to conclude that the experimentally observed permeabilization of membranes must be due to membrane-bound Aβ oligomers, and not monomers.

1. Introduction

Alzheimer's disease (AD) is a neurodegenerative disorder associated with synaptic loss, abnormalities in functioning of neurons, neuronal cell death and extracellular accumulation of senile plaques composed of the neurotoxic amyloid-β peptide (Aβ) [1,2]. Aβ is derived from the amyloid precursor protein (APP), a type-1 membrane integral glycoprotein through sequential cleavage by β- and γ-secretases [3]. The major alloforms of Aβ are $A\beta_{40}$ and $A\beta_{42}$, which differ by the presence of two amino acids, I41 and A42 at the C-terminus of the latter. The more hydrophobic $A\beta_{42}$ is the prevalent alloform seen in amyloid plaques, and has a greater tendency to aggregate into fibrils and plaques [4,5]. There is appreciable evidence suggesting that Aβ exerts its cytotoxic effect by interacting with membranes of neurons and other cerebral cells, such as astrocytes, microglial and cerebral endothelial cells [6,7]. A potential pathway for Aβ toxicity lies in its ability to alter biophysical membrane properties [8–11]. Aβ aggregates cause membrane disruption and increased permeability, allowing excessive leakage of ions, particularly calcium ions [12]. This imbalance in calcium homeostasis promotes neuronal excitotoxicity [12,13]. $A\beta_{42}$ oligomers interact with lipid raft related ganglioside GM1, further accelerating the amyloidogenic processing of APP [14].

Various experimental studies investigating the interactions between Aβ and phospholipids have revealed that Aβ prefers to bind to negatively charged lipids compared to zwitterionic lipids [15–17]. It has been shown that the enhanced association of Aβ with anionic lipid membranes leads to the insertion of Aβ into the membrane [15–17] and induces the formation of β-sheets [15,17–19] and Aβ fibrils [19–21]. NMR spectroscopy studies on $A\beta_{40}$ in a membrane-mimicking environment concluded that the peptide is unstructured in the N-terminal region from residues 1–14 and that the C-terminal hydrophobic residues from 15 to 36 adopt an α-helical conformation with a kink at residues 25–27 [22]. This kink may be significant in membrane insertion and conformational rearrangements [22]. Coles et al. proposed three possible models corresponding to different Aβ insertion depths in the membrane based on structural findings for $A\beta_{40}$ [22]. The two experimentally determined insertion depths have K28 and V24, respectively, at the membrane–water interface [22,23]. A third proposed model is with K16 at the membrane–water interface, where the entire α-helical conformation adopted by $A\beta_{40}$ (residues 15–36) spans the plasma

* Corresponding author at: Research Centre Jülich, Institute of Complex Systems: Structural Biochemistry, 52425 Jülich, Germany. Tel.: +49 2461 613670.
E-mail address: b.strodel@fz-juelich.de (B. Strodel).

0005-2736/$ – see front matter © 2012 Elsevier B.V. All rights reserved.
http://dx.doi.org/10.1016/j.bbamem.2012.09.001

membrane [22]. A study on soluble and aggregated forms of $A\beta_{40}$ on rat cortical synaptic plasma membrane using small angle X-ray diffraction and fluorescence spectroscopy showed that the monomer penetrates into the hydrophobic core of the bilayer, whereas the aggregated form was found interacting with the phospholipid headgroups [24]. Similarly, soluble $A\beta_{42}$ was found to intercalate the membrane of giant unilamellar vesicles composed of 1-palmitoyl 2-oleoyl phosphatidylcholine (POPC) or POPC/sphingomyelin (SM)/cholesterol (Chol), altering permeability properties of the bilayer [25]. However, permeabilization of lipid bilayers can also be caused by soluble amyloid oligomers [26]. NMR, CD, fluorescence and monolayer studies on $A\beta_{42}$ inserted into a POPC/POPS (palmitoyl-oleoyl phosphatidylserine) bilayer showed reduction in membrane stability with an increase in membrane fluidity [27]. This study also indicated that $A\beta_{42}$ alone could destabilize the membrane integrity in absence of ions, and that the peptide adopts a β-sheet structure in the membrane with increase in β content when Cu^{2+} is added [27]. Further experimental work carried out on $A\beta_{40}$ inserted into a zwitterionic phosphatidylcholine bilayer revealed that the perturbation of the bilayer integrity is caused by short β-sheet assemblies embedded in the lipid bilayer [28]. Atomic force microscopy of $A\beta_{42}$ [29] and $A\beta_{40}$ [30] in reconstituted membranes revealed ion-channel-like structures, which are able to cause cellular ionic imbalance [30–34]. Lal and coworkers also demonstrated through biochemical analysis that $A\beta$ forms stable tetramers and hexamers in lipid membranes [29].

It was shown that theoretical approaches are needed as a complement to experimental studies probing the principles governing $A\beta_{42}$ aggregation and $A\beta$–membrane interactions [35,36]. Various computational studies of $A\beta$ interacting with lipids have been performed to gain structural information at an atomistic level [37–59]. An atomistic model of $A\beta$ channel structures developed by Nussinov and coworkers provided information about the $A\beta$ conformation in membranes and ion-channel activity [37,38]. In another study they found that the channels break into mobile β-sheet subunits, which enable toxic ionic flux [39]. Strodel and coworkers also proposed $A\beta$ pore models composed of tetrameric to hexameric $A\beta$ subunits, which are similar to the models suggested by Nussinov and coworkers [46]. In [47] the stability of transmembrane β-barrel structures, each composed of eight $A\beta$ fragments $A\beta_{25-35}$, was investigated. Molecular dynamics (MD) studies of $A\beta_{40}$ inserted in a dipalmitoyl phosphatidylcholine (DPPC) bilayer with the peptide positioned with either K28, V24 or K16 at the membrane–water interface showed that in either case the peptide remained partially embedded in the membrane [48]. Loss of α-helicity in favor of β-strands was observed when the peptide was inserted at K28 and V24, whereas with K16 at the interface α-helicity was retained. For the deeper insertion depths, water molecules were seen entering the hydrophobic core accumulating near the charged residues of the peptide within the bilayer. It has also been reported that $A\beta_{40}$ causes DPPC lipid headgroup disorder and reduces the membrane thickness around $A\beta$ [49]. In a recent study, Lemkul and Bevan explored the interactions between $A\beta_{40}$ and several pure and mixed model membranes, and lipid rafts, both with and without GM1 [50]. $A\beta_{40}$ remained inserted in the membranes without GM1, but in several instances exited the raft containing GM1 initiated through hydrogen bonding of $A\beta_{40}$ with GM1. Another study on $A\beta_{40}$ preinserted in a DPPC bilayer found the peptide exiting the membrane and adsorbing to its surface, with helix conformation being the major secondary structure observed in the membrane-adsorbed $A\beta$ structure [54]. In a recent MD simulation study, the self-assembly of $A\beta$ in a mixed DPPC/cholesterol bilayer was investigated, uncovering the formation of a short parallel β-sheet between two peptides [59].

In the present MD study, we report the behavior of $A\beta_{42}$ preinserted into zwitterionic POPC and DPPC bilayers, and anionic 1-palmitoyl 2-oleoyl phosphatidylglycerol (POPG) bilayers. Here, our focus is on membrane-spanning structures based on the observation that $A\beta$ can form pore-like structures in reconstituted membranes [30–34]. Due to conflicting experimental results as to whether $A\beta$ is in a helical or in a β-sheet conformation in a lipid bilayer, we considered both transmembrane conformations as starting structures for our MD simulations in order to investigate whether the secondary structure leads to different behavior of the membrane-inserted $A\beta_{42}$ peptide. We used a β-sheet structure (monomer and tetramer) obtained from a global optimization approach [46] and a helix structure from an NMR study in an apolar solvent [22]. During each of the 500 ns MD simulations, $A\beta_{42}$ remains embedded in the lipid bilayer. We discuss our results in terms of structural stability of $A\beta_{42}$ and its effects on membrane functionality.

2. Methods

2.1. Starting structures

The two initial membrane-spanning $A\beta_{42}$ structures are a β-sheet and a helical conformation. The transmembrane β-sheet was obtained from a study for the $A\beta_{42}$ monomer and small oligomers using a global optimization approach in an implicit membrane model [46]. In this structure, the more hydrophobic C-terminal region starting from residue 17 is fully inserted into the hydrophobic membrane core, forming an antiparallel β-sheet with two turn regions, the first ranging from residues 23 to 29 and the second one involving residues 37 and 38. The first turn is prominent in many $A\beta$ structures identified from experiment [60–63] and simulation [64–66]. However, each of these models predicts a distinct turn structure. Ma and Nussinov independently predicted that the $A\beta$ peptide amyloid adopts a U-turn β-strand–loop–β-strand motif [66], qualitatively agreeing with the Tycko et al. model [63]. Lührs et al. [62] presented a 3D structure of $A\beta_{17-42}$ fibrils with a U-turn bent β-sheet based on hydrogen/deuterium-exchange NMR data, which further validates the computational model of Ma and Nussinov [66] and is consistent with the experimental model of Petkova et al. [63]. All these models, including our β-hairpin structure [46] share the key structural features of the salt bridge between Asp23 and Lys28 and the intramolecular hydrophobic cluster between Leu17/Phe19 and Ile32/Leu34. We decided to use our β-hairpin model as starting structure as it also provides a structural model for the more hydrophilic residues 1–16, which form a β-hairpin outside the membrane [46]. We study this transmembrane β-sheet as monomer (denoted SHEET in the following) and tetramer as obtained in [46] (Fig. 1a and b). The α-helical starting structure was obtained from an NMR study of $A\beta_{40}$ in an apolar solvent (PDB ID: 1BA4) [22]. We extended the 40 residue peptide to $A\beta_{42}$ by adding the two hydrophobic residues I41 and A42 in a coil conformation. Our motivation behind this extension was to study the role of the extra I41 and A42 residues in peptide–lipid interactions and the resulting structural changes in the peptide and membrane. Previous studies revealed an increased stability provided by I41 and A42 to the antiparallel β-sheet when compared to $A\beta_{40}$ [67]. Furthermore, by using the same peptide we wanted to be able to compare our findings for the helical and β-sheet transmembrane structures. The helical structure was studied for two insertion depths: (i) with K16 (denoted HEL-16) and (ii) with D23 (denoted HEL-23) at the membrane–water interface (Fig. 1c and d). Note that this nomenclature refers to the initial condition only as no restraints are imposed on the peptide. This implies that during the MD simulations the peptide can experience secondary structure changes and/or transpositions within the lipid bilayers so that the final state of an MD run does not necessarily correspond to the initial notation.

All our simulations were carried out at physiological pH giving rise to charge −3 for $A\beta_{42}$ with His residues modeled uncharged, Asp and Glu negatively charged, and Lys and Arg assumed being protonated. Our choice of the protonation state for the ionizable residues was based on their pK_a values as a function of depth in the membrane [68]. At pH 7, Lys and Arg become deprotonated only when they are in close vicinity to the membrane center, while the pK_a values of Asp and Glu rise above 7 inside the membrane core. In our simulations $A\beta_{42}$ is positioned such that K16, E22, D23 and K28 are at the membrane–water interface. Therefore, we assumed positive charges for

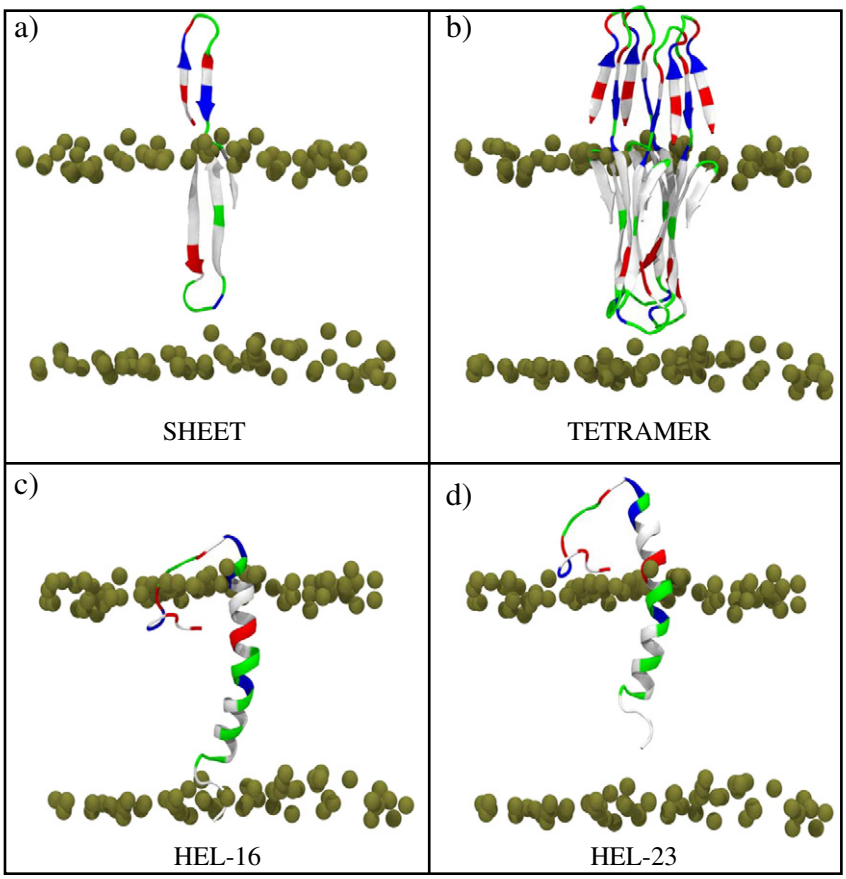

Fig. 1. Initial structures for the MD runs: (a) β-sheet monomer (SHEET), (b) β-sheet tetramer, (c) α-helix inserted with K16 at the membrane–water interface (HEL-16), (d) α-helix inserted with D23 at the membrane–water interface (HEL-23). The peptide is shown in cartoon and colored based on the physicochemical properties of the residues: blue, basic; red, acidic; white, hydrophobic; and green, polar. The bilayer phosphorus atoms are shown as Van der Waals spheres in tan color. Lipid tails and water molecules are not shown for clarity.

K16 and K28, and negative charges for E22 and D23. While this choice for Lys is undoubted, E22 and D23 are borderline cases as their protonation state could change during the MD simulation. Ideally, one would like to perform constant pH MD simulations. Such a method was recently implemented into GROMACS for explicit water simulations [69], which is, however, not available yet for simulations including lipid bilayers. The N- and C-terminals were capped to nullify the effect of terminal residues in peptide–lipid interactions.

2.2. Molecular dynamics simulations

All MD simulations were performed with the GROMACS 4.0 package [70]. The Aβ_{42} peptide was described using the GROMOS96 53A6 force field [71], and the lipids were modeled with modified Berger force field parameters for use with the GROMOS96 53A6 force field [72]. Recently, we demonstrated that the GROMOS96 53A6 force field is able to correctly model the structural propensities of Aβ_{40} and Aβ_{42} [73]. Initial coordinates of 128 lipids for POPC, DPPC and POPG bilayers equilibrated with water for 40 ns were obtained from Kukol's work on lipid models [72]. We performed 100 ns MD simulations of the pure lipid bilayers for comparison with our simulations involving Aβ_{42}. For the latter, Aβ_{42} was inserted into the pre-equilibrated lipid membrane using the INFLATEGRO script [74]. Once Aβ_{42} was inserted into the lipid membrane, the structures were solvated with SPC water molecules, Na^+ counterions were added to balance the peptide and POPG charge, and 0.1 M NaCl salt was added to bring the system to a near physiological salt concentration. The simulations were carried out in a $65\times65\times95$ Å^3 box. An initial equilibration under isothermal–isochoric conditions was performed for 100 ps during which the protein heavy atoms and phosphorous atoms of the lipid headgroups were restrained with a force constant of 1000 kJ mol^{-1} nm^{-2}. Here, the v-rescale thermostat with a coupling constant of 0.1 ps was used to regulate the temperature of the peptide, lipids, and solvent/ions separately at 298 K for the POPC and POPG simulations, and at 325 K for the DPPC simulations. The higher simulation temperature for DPPC is necessary for the membrane to remain fluid, which is already guaranteed for POPC and POPG at 298 K. The systems were then equilibrated under isothermal–isobaric (NPT) conditions for 30 ns. For the NPT ensemble the Nose–Hoover thermostat was used to regulate the temperature along with semiisotropic Parrinello–Rahman pressure coupling. The bilayer normal *z*-direction and *xy*-plane were coupled separately with a time constant of 5.0 ps maintaining a constant pressure of 1 bar in all directions. An isothermal compressibility of 4.5×10^5 bar^{-1} was applied in all box dimensions. Long-range electrostatics were calculated using the Particle Mesh-Ewald method in connection with periodic boundary conditions. Van der Waals and Coulombic interaction cutoffs were set to 12 Å and the LINCS algorithm was used to constrain all bond lengths. Following equilibration, production MD runs were performed for 500 ns for each system. Here the parameter settings were similar to the NPT equilibration step, except that all restraints were removed and the time constant for pressure coupling was set to 2.0 ps for maintaining a constant pressure of 1 bar. The time step for integration was 2 fs, with coordinates and velocities saved every 20 ps for analysis.

2.3. Analysis

The structural stability of Aβ_{42} was analyzed separately for the N-terminal residues outside the membrane and the C-terminal residues

inside the hydrophobic bilayer core. For Aβ_{42} inserted at K16, the N-terminal residues thus range from 1 to 16 and the C-terminal residues from 17 to 42, whereas for Aβ_{42} with D23 at the membrane–water interface residues 1–23 and residues 24–42 were considered as N- and C-terminal segments, respectively. The secondary structure of Aβ_{42} was analyzed using the DSSP (dictionary of protein secondary structure) method [75]. The tilt angle of the peptide inside the bilayer core relative to the membrane normal and motion of the peptide along the membrane normal was calculated using GROMACS analysis tools. Water permeation across the membrane was quantified using VMD [76]. The probability of hydrogen bond (H-bond) formation, either between peptide and water or between peptide carbonyl and amide groups, was considered based on a cutoff distance of 3.6 Å between donor and acceptor atoms and a cutoff angle off linearity of 30°. We used the grid-based membrane analysis tool GRIDMAT-MD to calculate the area per lipid and the bilayer thickness [77]. For the bilayer thickness we report phosphate-to-phosphate (P–P) distances. To characterize the effects of the peptide on the orientational mobility of the lipid molecules we calculated the lipid tail order parameter S_{CD} defined as

$$S_{CD} = \left\langle \frac{3\cos^2\theta - 1}{2} \right\rangle , \quad (1)$$

where θ is the angle between the C – H bond vector (in the simulation) or the C – D bond vector (in the experiment) and the bilayer normal. The angular brackets indicate averaging over lipids and over time.

3. Results and discussion

In all cases Aβ_{42} remained inside the bilayer throughout the MD simulations on the sub-microsecond scale. This finding is independent of the secondary structure of the starting conformation and the lipid bilayer type. The final structures after 500 ns of MD simulations of the SHEET, HEL-16, HEL-23 starting structures in a POPC, DPPC and a POPG bilayer are presented in Fig. 2. These figures show that the N-terminal segment of the peptide is generally adsorbed to the bilayer surface of the upper leaflet as a result of electrostatic interactions and hydrogen bonding. These interactions rupture the lipid packing and lead to a tilt of the lipids around the peptide, allowing passage of water molecules into the hydrophobic core of the bilayer. The peptide residues, rendered as pink spheres in Fig. 2, are those involved in H-bond formation with the water molecules entering the bilayer. This is a measure of how deep water molecules can enter the hydrophobic core once they have passed the head group region and can form H-bonds with the transmembrane part of Aβ_{42}. It should be noted, however, that this does not indicate that the water molecules also translocate the membrane. Water translocation was considered only when a water molecule passed both headgroup regions, and not when it entered and exited at the same side of the bilayer. In the Supporting material the change of residual secondary structure during the MD simulations is presented (Figs. S1–S4). Our analysis of the MD trajectories showed that all Aβ_{42} structures considered are relatively stable on the time scale of the simulations in terms of their overall position in the bilayer and with regard to their secondary structure. We, therefore, show the final MD states as representative structures in Fig. 2.

In order to establish what kind of variations are to be expected for a system when simulated multiple times, we repeated the simulation of the SHEET in POPC two more times. These MD simulations were initiated from the same starting structure (Fig. 1a) yet with different initial velocity distributions. The final structures of the three 500 ns MD simulations of SHEET in POPC are shown in Fig. S5a, while in Fig. S5b the corresponding secondary structure analysis is presented. It can be seen that in all three cases the transmembrane β-sheet is stable and does not move considerably along the membrane normal. Only the structures of the N-terminal residues outside the membrane are different resulting from the combined action of electrostatic interactions between charged N-terminal Aβ_{42} residues and lipid headgroups, a high preference for random coil structures of the N-terminal residues in water, and stochastic conformational changes associated with thermal movements. However, in all three cases the N-terminus of Aβ_{42} is attracted by the membrane surface. The analysis of the effects of the SHEET structure on the POPC bilayer revealed very similar results for these three MD simulations, too. These findings allow us to conclude that structural changes of SHEET inside the membrane core are mainly a result of statistical fluctuations around the stable β-sheet structure, which is likely to be stable on a much longer time scale, while the structure of the N-terminus would probably change further when simulated for longer. Depending on the lipid type and initial Aβ_{42} structure, transmembrane Aβ_{42} displays different stabilities, which will be discussed in the following, where effort was made to address whether observed instabilities are inherent and likely to be more pronounced on a longer timescale.

3.1. Effects of transmembrane Aβ_{42} on lipid bilayers

From our MD simulations we found that the effects of transmembrane Aβ_{42} monomer on the bilayers depend more on the lipid type than on the inserted Aβ_{42} structure. The analysis of the bilayer properties is summarized in Table 1. This table lists the area per lipid and bilayer thickness, the average number of H-bonds between Aβ_{42} and water molecules in the bilayer core, the number of intrapeptide H-bonds (including interpeptide H-bonds in case of the Aβ_{42} tetramer) in the bilayer core, the number of water molecules passing the membrane in the vicinity of Aβ_{42}, and the average motion of Aβ_{42} along the bilayer normal. In Figs. S6 and S7 images of the bilayer thickness calculated for the final states of the MD simulations are shown. In almost all cases we observed that the upper leaflet has a lower area per lipid headgroup than the lower leaflet. However, both the upper and lower leaflets have a decreased area per lipid headgroup when compared to the bilayers without peptide. This area contraction results from attractive electrostatic forces and H-bonds between Aβ_{42} residues and lipid headgroups. For the bilayer thickness we find that the average thickness of POPC and POPG bilayers is hardly affected by embedded Aβ_{42} with thickness changes less than 1 Å. However, Fig. S6 reveals that the POPC, POPG and DPPC thicknesses around Aβ_{42} are decreased in order to improve the hydrophobic matching between bilayer and Aβ_{42}, whose hydrophobic width is smaller than those of the lipids (i.e., negative hydrophobic mismatch). The three bilayers studied exhibit a similar thickness of about 25–30 Å in the neighborhood of the peptide, which corresponds to the hydrophobic width of the latter for both β-sheet and helical structures. This implies that the thinner region close to Aβ_{42} is compensated by an increase in thickness further away from the peptide [49,78] as evidenced by Figs. S6 and S7. This effect is most pronounced for DPPC, for which we observe P–P distances reaching up to 50 Å (Fig. S6), corresponding to an increase of average thickness by 3–4.5 Å, when compared to the peptide-free bilayer.

An increased bilayer thickness results from increased lipid chain order. We therefore calculated the order parameter S_{CD} of acyl chain 1 (sn-1) separately for the POPC, DPPC and POPG lipids within 5 Å of Aβ_{42}, and for the lipids, which are more than 5 Å away from Aβ_{42}. We chose sn-1 because this acyl chain is identical for POPC, DPPC and POPG guaranteeing comparability. The results of this analysis are shown in Fig. 3. For comparison we also present S_{CD} of sn-1 of the pure POPC, DPPC and POPG bilayers obtained from 100 ns MD runs of the peptide-free lipid bilayers. The lipid order is generally decreased around the peptide as the corresponding S_{CD} value is smaller than the one for the peptide-free bilayer, while lipid order is increased for the lipids further away from the peptide. This effect is most pronounced for Aβ_{42} in DPPC, which is in agreement with the marked increase of the DPPC bilayer thickness with increasing

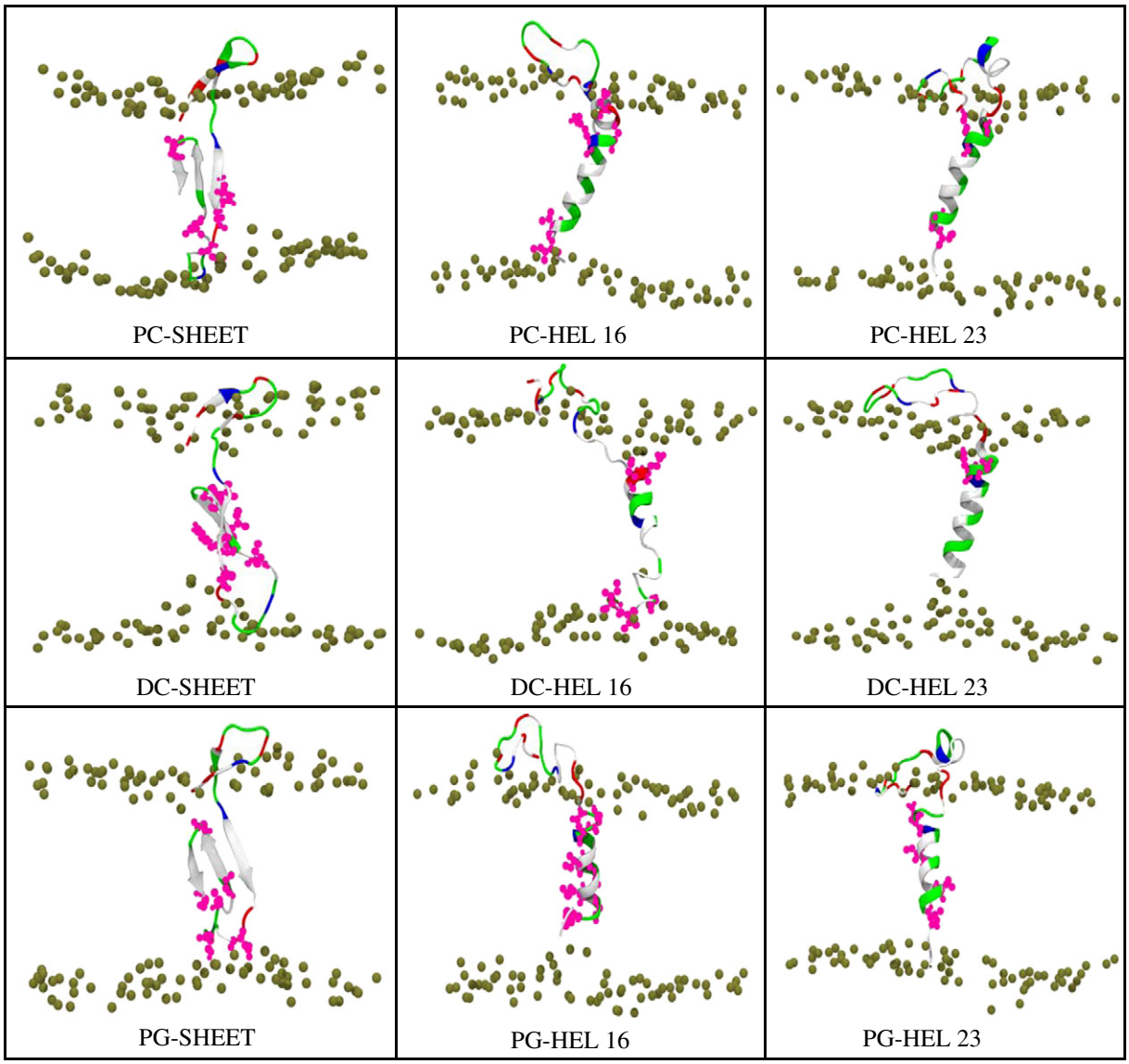

Fig. 2. Final states after 500 ns MD simulations of Aβ_{42} in POPC (PC), DPPC (DC) and POPG (PG) bilayers. For coloring explanation see Fig. 1. Peptide residues marked with pink spheres are involved in H-bond formation with water molecules entering the bilayer.

distance to the peptide. This behavior can be explained by the saturated acyl chains, which are less able to adapt to the peptide than lipids with unsaturated chains [78]. SHEET and HEL-23 inflict the largest ordering effect on DPPC with HEL-23 already increasing the lipid order for the lipids within 5 Å of Aβ_{42}. The corresponding plot of the bilayer thickness (Fig. S6) shows that only the lipids very close to HEL-23 are markedly disordered. In POPC the (dis)ordering effect of Aβ_{42} on the lipids is smallest. Only for the middle section of the sn-1 chain in POPC, which is close to the double bond of the unsaturated sn-2 acyl chain, the lipid tail order is increased for the lipids greater than 5 Å away from the peptide. In POPG the disordering effect for lipids within 5 Å of the peptide is more pronounced than in POPC, which is due to the repulsive interactions between the negatively charged head groups and the negative charges in the N-terminal part of Aβ_{42}. A similar impact on acyl chain order and bilayer thickness was observed for negatively mismatched transmembrane helices [79] and helical Aβ_{40} in a DPPC bilayer [49]. Thus, our simulation results show that Aβ_{42} inserted as monomeric or tetrameric β-sheet leads to a similar bilayer perturbation as membrane-embedded helical Aβ_{40} [49].

3.2. The transmembrane SHEET structure

In the SHEET structure, the negatively charged residues E22 and D23 cause the lipid headgroups of the lower leaflet to be shifted upwards into the hydrophobic core resulting from interactions with the headgroups, thereby facilitating the entry of water molecules from the bottom of the bilayer. Most of these water molecules remain in the vicinity of the charged Aβ_{42} residues within the membrane. However, the water molecules can also form H-bonds with peptide carbonyl and amide groups, which are not involved in intrapeptide H-bonds. The results in Table 1 show that, irrespective of the bilayer type, the SHEET structure forms more H-bonds with water molecules and fewer intrapeptide H-bonds compared to the helical structures under study. Therefore, hydrophobic residues can also interact with water inside the hydrophobic bilayer core via H-bond formation as indicated by the pink spheres in Fig. 2. However, the translocation of water molecules depends on the lipid type, not the number of water molecules crossing the headgroup region. For instance, while there are, on average, 18 and 19 H-bonds between Aβ_{42} and H_2O molecules for

Table 1
Effects of $A\beta_{42}$ on lipid bilayers in terms of area per lipid headgroup, bilayer thickness, number of translocated water molecules, number of H-bonds between $A\beta_{42}$ and water in the hydrophobic membrane core, number of H-bonds between peptide carbonyl and amide groups (i.e., intrapeptide H-bonds for for SHEET, HEL-16 and HEL-23; intra- and interpeptide H-bonds for the tetramer), and the motion of the center of mass of $A\beta_{42}$ along the membrane normal with respect to its initial value at the start of the MD run. For the simulations of the pure lipid bilayers, average values were obtained from 100 ns MD simulations starting from bilayers from previous 40 ns MD runs [72]. For the results with $A\beta_{42}$, average values were calculated for the last 400 ns of the 500 ns MD simulations. Only for the water translocation all occurrences during each of the 500 ns MD simulations are reported.

$A\beta_{42}$ structure	Bilayer	Area per lipid [Å^2]		Bilayer	Translocation	H-bonds		$A\beta_{42}$ motion along z [Å]
		Top leaflet	Bottom leaflet	thickness [Å]	#H_2O	$A\beta_{42}/H_2O$	CO/NH	
Peptide-free	POPC	69.3[a]	69.3	35.1	1[b]	n/a	n/a	n/a
SHEET		62.6	63.4	35.5	1	18	10	2.6
HEL-16		63.4	67.5	35.4	1	6	12	8.9
HEL-23		65.2	68.5	35.0	3	3	13	−5.3
Tetramer		62.0	65.3	34.9	5	95	50	5.1
Peptide-free	DPPC	62.3[a]	62.3	37.1	4[b]	n/a	n/a	n/a
SHEET		53.7	54.5	41.5	20	19	9	−0.5
HEL-16		50.9	56.6	40.3	16	18	10	4.6
HEL-23		51.8	57.1	41.6	13	2	14	1.9
Peptide-free	POPG	70.0[a]	70.0	34.8	1[b]	n/a	n/a	n/a
SHEET		69.3	69.3	34.5	2	13	8	−3.7
HEL-16		64.0	69.7	34.3	1	9	10	9.0
HEL-23		64.0	68.7	34.5	1	9	10	−6.4

[a] The experimental values for the area per lipids of the peptide-free bilayers are: POPC, 68.3 Å^2 [92]; DPPC, 64.0 Å^2 [93]; and POPG, 67.3 Å^2 [94].
[b] The number of H_2O molecules passing the peptide-free bilayers was obtained from 100 ns MD simulations while those involving $A\beta_{42}$ from 500 ns MD simulations.

SHEET in POPC and DPPC, respectively, only one water molecule is able to cross the POPC bilayer. This is far less than the 20 water molecules translocating through the DPPC bilayer within the 500 ns simulation.

Depending on the lipid type, we observe almost none to minor loss of β-strands in the hydrophobic core of the bilayer (Figs. 2 and S1–S3). We find the SHEET structure to be most stable in POPC and least stable in DPPC. In the three simulations of SHEET in POPC, the largest change we observed was a slight upward motion of the whole peptide by 2 to 3 Å. In order to analyze how much the salt bridge between D23 and K28 helps stabilize the transmembrane SHEET, we calculated the distance between the anionic carboxylate of either E22 or D23 and the cationic ammonium from K28 (Fig. S8). In none of the bilayers a salt bridge between E22 and K28 exists. It can be seen that a salt bridge between D23 and K28 is formed only in POPC, while in DPPC and POPG this salt bridge is not present. This observation correlates well with the high SHEET stability observed in POPC. In the DPPC simulation the SHEET structure becomes unstable because of the missing salt bridge leading to a widening of the turn between residues 23 and 29. Instead, E22 and D23 interact with the headgroups of the lower leaflet, leading to further destabilization of the SHEET structure in DPPC: the peptide unfolds from β-sheet to coil and bend structures, except for residues L17–F20, L34–V36, V40 and I41. In DPPC the SHEET structure hardly moved along the membrane normal (see Table 1). In the simulation with POPG, we observe a transient loss of β-sheet to coil from residues L17 to A21, and from sheet-turn-sheet to sheet-bend-coil for residues G33 to I41 during the initial 170 ns of the MD run. However, for the remainder of the MD simulation the β-sheet has reformed and is considerably stable despite the missing D23–K28 salt bridge. Due to electrostatic repulsion between the negatively charged N-terminal $A\beta_{42}$ part and the negatively charged headgroup region, the peptide was pushed deeper into the membrane by about 3.7 Å.

3.3. Helical $A\beta_{42}$ with K16 at the membrane–water interface (HEL-16)

The simulations of HEL-16 were performed for comparison with the SHEET structure, which has K16 at the membrane–water interface. A key finding for HEL-16 in POPC and POPG is that the peptide moves considerably upwards, i.e., by 8.9 Å and 9.0 Å respectively. This vertical motion is driven by the considerable reduction in free energy when removing the charged residues E22 and D23 from the hydrophobic core [68], leading to the alignment of these two residues with the bilayer–water interface. It thus follows that HEL-16 becomes identical to the HEL-23 conformation in the course of the POPC and POPG simulations. The negative headgroup charge in POPG leads to a stronger influx of water into the membrane as shown by the higher number of H-bonds between $A\beta_{42}$ and H_2O in POPG compared to

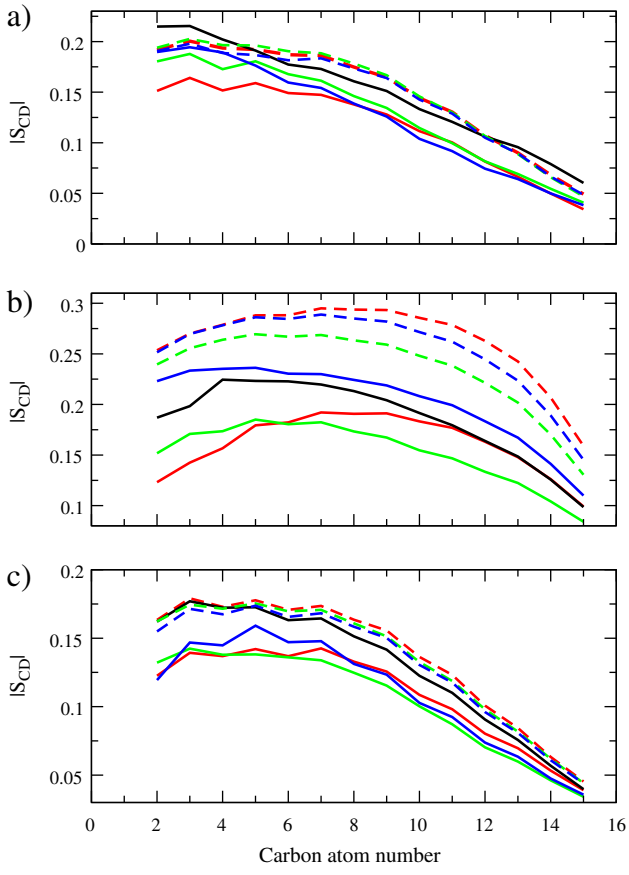

Fig. 3. Time-averaged (over the last 400 ns of the MD simulations) order parameter S_{CD} of the sn-1 chain of (a) POPC, (b) DPPC, and (c) POPG lipids. Results are shown for SHEET (red), HEL-16 (green) and HEL-23 (blue) and are distinguished for the lipids within 5 Å of $A\beta_{42}$ (solid) and for the lipids >5 Å away from $A\beta_{42}$ (dashed). For comparison, S_{CD} of the sn-1 chain obtained from 100 ns MD runs of peptide-free lipid bilayers is also presented (black).

POPC (Table 1). However, in both POPC and POPG we find only one H_2O molecule translocating through the membranes in the vicinity of Aβ_{42}. In the POPC bilayer, water molecules entering the upper leaflet mainly interact with residues E22–S26 around the headgroup region, whereas water molecules entering the lower leaflet interact with the C-terminal residues G37–A42. Conversion of the α-helix to turn structure is found for residues D23–S26, which are inside the membrane in the vicinity of the headgroup region interacting with water. A high stability of the transmembrane helical structure is seen for residues N27–V39, which are well placed within the hydrophobic core. The last three residues, V40–A42, retained their coil structure and caused the lower lipid headgroups to slightly shift upwards.

In POPG only residues K28–G37 of HEL-16 remain α-helical, while the other residues adopt coil and turn conformations. We can thus conclude that the helix in POPG is less stable than in POPC, which is confirmed by the fewer intrapeptide H-bonds in POPG (Table 1). Another interesting observation is that HEL-16 in POPC is more strongly tilted with an average tilt angle of 20°, while in POPG the tilt angle is only 13°. This difference cannot be explained by the hydrophobic mismatch between Aβ_{42} and the membranes as (i) the hydrophobic mismatch is the same for POPC and POPG; and (ii) an increased tilt angle is commonly found for positive hydrophobic mismatch between transmembrane helices and lipid bilayers to fully incorporate the hydrophobic peptide residues into bilayers [79]. We therefore conjecture that the different tilt angles observed for HEL-16 in POPC and POPG originate from the different head groups (see Section 3.5).

In case of HEL-16 in a DPPC bilayer, the α-helical structure is only stable between residues A21 and A30, whereas the other residues inside the DPPC membrane (K16–F20 and I31–A42) unfold to turn and bend structures (Figs. 2 and S1) leading to fewer intrapeptide H-bonds compared to HEL-16 in POPC. A considerable amount of water molecules is able to enter the hydrophobic bilayer region as evidenced by the large number of H-bonds between Aβ_{42} and H_2O (Table 1). While many of the water molecules remain in the vicinity of the headgroup regions and mainly interact with residues V18–D23 and G37–A42, we observe an increased water flow through the DPPC membrane in the vicinity of HEL-16. During the 500 ns MD simulation, 16 H_2O molecules traversed the bilayer, i.e., four molecules fewer than for SHEET in DPPC but markedly more than for HEL-16 in POPC and POPG. A further difference to the POPC and POPG simulations is that HEL-16 in DPPC does not move upwards leaving E22 and D23 inside the hydrophobic core, which induces helix-to-coil transitions in Aβ_{42}.

3.4. Helical Aβ_{42} with D23 at the membrane–water interface (HEL-23)

HEL-23 in POPC and POPG bilayers moved downwards by 5.3 Å and 6.4 Å, respectively. This downward motion leaves the negatively charged residues E22 and D23 in the upper headgroup region, but allows a reduced negative mismatch between Aβ_{42} and the bilayers. HEL-23 in DPPC, on the other hand, moves somewhat upwards by 4.6 Å. Here, the lipids around HEL-23 in the lower DPPC leaflet have moved upwards to compensate for the negative hydrophobic mismatch. Nonetheless, the final structures in Fig. 2 show that the vertical location of HEL-23 in POPC, DPPC and POPG is very similar.

The transmembrane α-helix of HEL-23 is relatively stable in all three bilayers (albeit to different degrees), whereas the residues outside the membrane lose their helicity in favor of disordered coil and turn conformations. Residues E22 and D23 interact strongly with the headgroups of the upper leaflet, causing headgroup disorder and a reduction of the area per lipid. As for HEL-16, HEL-23 displayed a larger tilt of 23° in POPC and a reduced tilt of only 13° in POPG. In POPC, the helix is stable within the membrane between residues V24–V39, which is also reflected in the relatively high number of 13 intrapeptide H-bonds. Most of the water molecules entering the bilayer interact with the peptide around the headgroup regions and do not penetrate deeply into the hydrophobic core. On average, there are only three H-bonds between Aβ_{42} and H_2O molecules in the POPC bilayer, while three water molecules were observed to cross the POPC bilayer with HEL-23 inserted in it. The comparison between HEL-16 and HEL-23 in POPC shows that both systems behave very similarly after 250 ns, at which time HEL-16 has already moved upwards, positioning E22 and D23 at the membrane–water interface. In the simulation with DPPC, HEL-23 retains its transmembrane α-helical structure, which is different from HEL-16 in DPPC, which was not stable. Even the terminal hydrophobic residues I41 and A42 fold from coil to α-helix in HEL-23, adding further to the stability of this structure. The high α-helical stability leads to 14 intrapeptide H-bonds and only two Aβ_{42}–H_2O H-bonds in the DPPC bilayer. It should be noted that the helix in HEL-23 in DPPC was stable despite the elevated simulation temperature of 325 K necessary in the DPPC simulations, compared with 298 K in the POPC and POPG simulations.

As for SHEET and HEL-16 in DPPC we also observe considerable water flow across the membrane for HEL-23 in DPPC though the translocation is somewhat reduced compared with the other two cases (i.e., 13 H_2O molecules versus 20 and 16, respectively). Our simulations of HEL-23 in POPG revealed a loss of the α-helix from residues L17 to N27, which instead adopt coil and turn conformations leading to only 10 intrapeptide H-bonds. On the investigated timescale, the α-helix is stable between residues K28 and G38. The last three residues extend to a coil structure reaching the bottom membrane surface, thereby disordering adjacent headgroups. Like in POPC, HEL-16 and HEL-23 behave very similarly in POPG after HEL-16 has moved upwards, bringing E22 and D23 in the headgroup area. This behavior includes stability, H-bond formation, water translocation and peptide tilt.

3.5. Mixed POPC/POPG bilayer simulations of HEL-23

To better understand the influence of the lipid type on the helical structures in POPC and POPG, we performed two more 100 ns MD simulations of HEL-23 in mixed POPC/POPG bilayers with asymmetric lipid distribution. The simulation of HEL-23 is also representative of HEL-16 as the latter becomes HEL-23 in POPC and POPG. The asymmetric lipid distribution was chosen such that in one simulation the upper leaflet was composed of only POPG lipids and the lower leaflet of only POPC lipids, while in the other simulation it was the other way round, i.e., POPC in the upper and POPG in the lower leaflet. The helical structure was preinserted with D23 at the membrane–water interface (HEL-23). The final structures after 100 ns of MD simulations are shown in Fig. 4a and b. The comparison of the POPC/POPG and POPG/POPC (here the order of the lipids refers to the upper and lower leaflets) results emphasizes the destabilizing effect of the anionic headgroups on the helix, when POPG is in the upper leaflet (Fig. 4b). In this region the helical structure is lost up to residue 26 in favor of coil structures, while the helix is stable between residues 15 and 38 in POPC/POPG. Residues 37 to 42 are in different coil conformations in the POPC/POPG and POPG/POPC simulations. These findings are in agreement with the results for POPC and POPG simulations, which also revealed a destabilizing effect of the lower headgroups on the vicinal helical Aβ_{42} residues. In both POPC/POPG and POPG/POPC Aβ_{42} is tilted by on average 23°, which is different to the smaller tilt in the POPG bilayer.

To better understand why HEL-23 (and HEL-16) stability and tilt angle differ in POPC and POPG, we looked more closely at the interactions of Aβ_{42} with adjacent lipids. Fig. 4c and d shows the final state of HEL-23 with the lipid and water molecules within 5 Å of the peptide for the POPC and POPG simulations, respectively. It is immediately obvious that more lipid molecules are in the direct neighborhood of Aβ_{42} in POPC than in POPG. The reduced lipid density in POPG, which is a result of electrostatic repulsion between the POPG headgroups, allows Aβ_{42} more orientational freedom inside the membrane. It can be seen that the POPC lipids around Aβ_{42} are more ordered than the POPG lipids, which is supported by our findings from the order parameter analysis

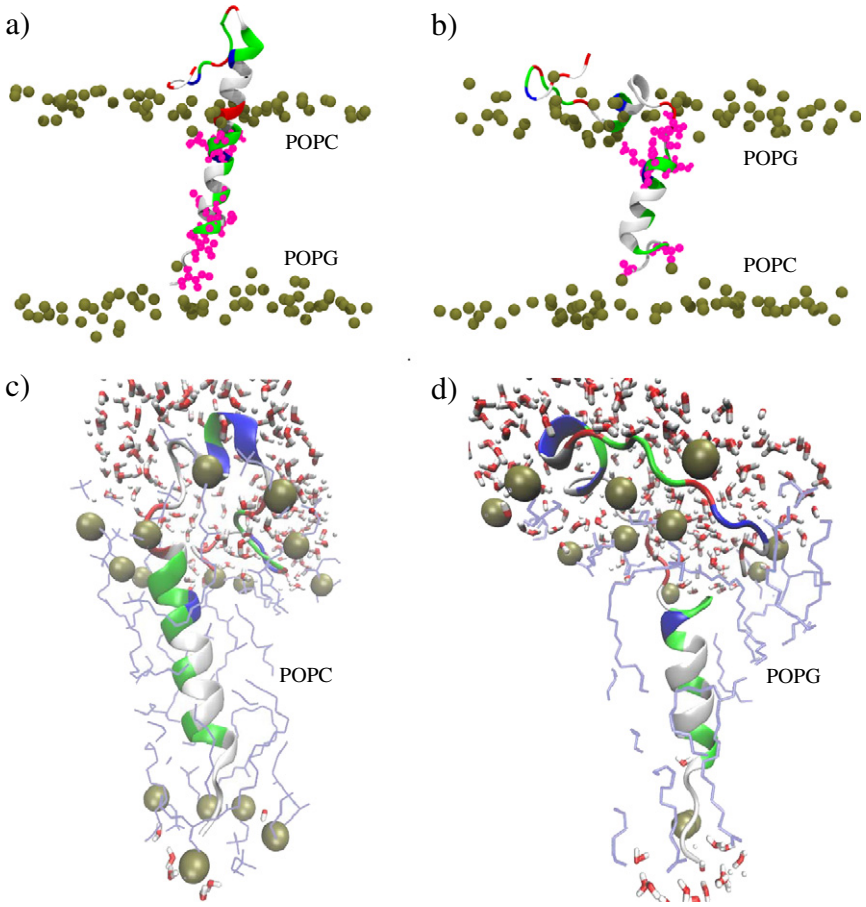

Fig. 4. Panels (a) and (b) show the final states after 100 ns MD simulations of HEL-23 in mixed POPC/POPG and POPG/POPC bilayers, respectively. Here, the order of the lipid type refers to the upper/lower leaflet. For coloring explanation see Fig. 1. Panels (c) and (d) show a close-up of the final states after 500 ns MD simulations of HEL-23 in POPC and POPG, respectively. The lipids (Van der Waals spheres in tan for phosphorus atoms, light-blue lines for lipid tails) and water molecules (licorice representation with red for oxygen atoms and white for hydrogen atoms) are shown within 5 Å of $A\beta_{42}$. For coloring explanation for $A\beta_{42}$ see Fig. 1.

in Fig. 3. The POPC lipid order seems to inflict a tilt on HEL-23 in POPC. The reduced lipid density around $A\beta_{42}$ in POPG allows more water molecules to enter the hydrophobic core, which induce helix-to-coil transitions in residues D23 to N27. The same happens in the lower POPG leaflet where one H_2O molecule interacts with V39 (Fig. 4d), thereby destroying the helical structure for this residue, while the helix for V39 in HEL-23 in POPC remains intact (Fig. 4c). Therefore, we can conclude that the reduced lipid density and increased lipid disorder around helical $A\beta_{42}$ in POPG, inducing water influx into the hydrophobic core, are responsible for the smaller tilt angle and larger structural instability of HEL-23 in POPG. Aside, it should be noted that in both POPC and POPG simulations a π-helix is sampled in the N-terminal region between V13 and K16, i.e., this helix seems to be a stable structural element for $A\beta$ adsorbed to the membrane surface [51,55].

The asymmetric bilayer composition leads to increased water permeation: within the two 100 ns MD simulations we observed two and one H_2O molecules traverse the POPC/POPG and POPG/POPC bilayers, respectively. On a 500 ns time scale this corresponds to on average 10 and 5 H_2O molecules, respectively. The increased water permeation in comparison to the symmetric one-component POPC and POPG bilayers can be explained by a nonzero net dipole moment of the asymmetric bilayers [80,81]. This asymmetry also seems to induce directional water flow from POPG to POPC, as observed for three traversing events of water molecules through the bilayers. However, it should be noted that this effect needs to be tested on a longer time scale. In general, the electrostatic potential of cell membranes is crucial for numerous membrane-mediated biological phenomena, such as the activation of voltage-gated membrane proteins, conductance of ionic channels, binding of therapeutic solutes to membranes, and trafficking across cell membranes [82].

3.6. The transmembrane β-sheet tetramer

Our motivation for studying the transmembrane β-sheet tetramer was to test whether it is more stable than the single transmembrane β-sheet and could thus serve as building block for a pore composed of several $A\beta_{42}$ β-sheet oligomers [37–39,46]. Furthermore, we wanted to investigate whether the $A\beta_{42}$ tetramer is able to disturb the lipid bilayer sufficiently in order to allow increased water translocation and ion passage through the membrane as found experimentally [26]. We performed the simulation for the β-sheet tetramer only in a POPC bilayer as the monomeric SHEET structure was most stable in this bilayer type. The final structure of this 500 ns MD simulation is shown in Fig. 5.

We observe that, unlike in the monomeric SHEET, the N-terminal β-hairpins are stable in the tetramer (see DSSP plot in Fig. S4). They interact with each other rather than with the bilayer surface, causing the N-terminal regions to stick out into the water instead of being adsorbed to the bilayer surface, as we observed for all monomeric transmembrane $A\beta_{42}$ structures. Along with the overall negative charge of the N-terminal

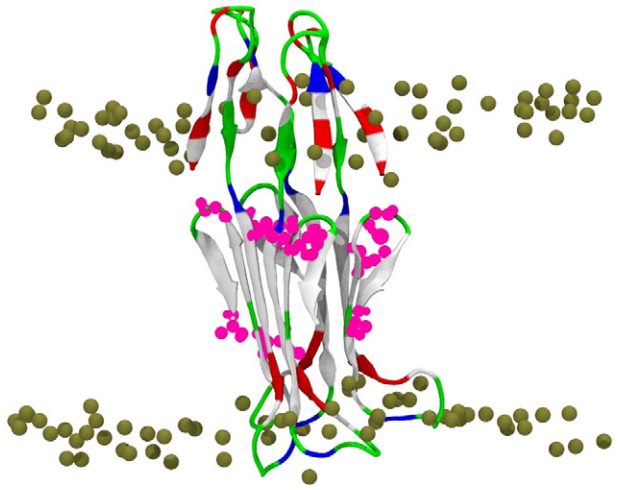

Fig. 5. Final state of the 500 ns MD simulation of the Aβ_{42} β-sheet tetramer in a POPC bilayer. For coloring explanation see Fig. 1.

half of the peptide, this structure might thus act as a funnel for cations to be inserted into the membrane in larger Aβ assemblies composed of our tetramer model [83]. The transmembrane β-strands were more stable throughout the simulations compared to the β-sheet monomer, which is also reflected in the increased number of intra- and interpeptide H-bonds per peptide, when compared to SHEET in POPC. The increased stability, resulting from favorable interpeptide interactions [46], leads to a decrease in peptide–lipid interactions as Fig. S9 supports. Water molecules enter the membrane in the upper and lower leaflets, and mainly interact with the negatively charged residues E22 and D23 around the lower lipid headgroup region and with polar residues near the upper headgroup region. Table 1 shows that, on average, there are 95 H-bonds between Aβ_{42} and water within the membrane, i.e., around 24 H-bonds per peptide. The tetramer thus allows more water to enter the POPC bilayer than the monomeric SHEET. It also leads to an increased membrane translocation when compared to monomeric Aβ_{42} in POPC, as five H_2O molecules were found to cross the bilayer within the 500 ns simulation.

From the last observation we can conclude that increased permeabilization of lipid bilayers due to Aβ can only result from transmembrane Aβ oligomers and not monomers, which is in agreement with experimental findings [26]. In the study by Glabe and coworkers it is further reported that Aβ_{42} oligomers increase the conductance of lipid bilayers, with the increase in conductivity being proportional to the concentration of oligomers [26]. They do not find any evidence for pore formation or ion selective conductance. Instead, soluble oligomers appear to enhance the ability of ions to move through the lipid bilayer on their own. While we have not observed the translocation of ions in our simulations, steady water permeation is a prerequisite for ions crossing the lipid bilayer through protein-facilitated diffusion. Hence, the β-sheet tetramer in our study is still too small or of the wrong conformation, as steady water flow could not be observed. The structure and size of the smallest Aβ oligomer facilitating the conductance of lipid bilayers remain to be elucidated. However, to our knowledge, our simulation study is the first one to address the permeabilization of lipid bilayers resulting from Aβ_{42}, employing a rigorous bottom-up approach (see Section 3.8). Previous simulations of membrane-embedded Aβ monomers report the entry of water molecules into the bilayer and interacting with charged residues in the C-terminal segment of the peptide, yet no water passage across the membrane was mentioned [48]. Nussinov and coworkers, on the other hand, used a top-down approach by constructing annular channels guided by NMR data for Aβ fibrils [62,63] and studied the stability and conductivity of such channels using MD [37–45].

3.7. Comparison of transmembrane Aβ_{42} in POPC, DPPC and POPG

Aβ_{42} in POPC and POPG bilayers behaved more similarly when compared to Aβ_{42} inserted in a DPPC bilayer. Possible explanations for this result are the larger length and the saturation of the hydrophobic tails in DPPC compared to POPC and POPG, and the higher temperature in the DPPC simulations. However, the anionic headgroup charges of POPG also influence the structural stability by inducing structural transformations to coil conformations in the membrane-inserted Aβ_{42} residues close to the headgroup regions. These findings apply to Aβ_{42} in the SHEET, HEL-16 and HEL-23 configuration. For the SHEET structure, we observed a broadening of the β-hairpin towards a U-shaped β-strand–loop–β-strand motif, which is in agreement with previous computational [37,38,66] and experimental [62,63] models. However, it should be noted that this structural model was found for the fibril. It remains to be demonstrated by means of experimental structure determination that the β-strand–loop–β-strand motif is also present in membranes [26]. Aβ_{42} inserted into a POPC bilayer as a β-sheet or helix is relatively stable within the membrane core, which is supported by experimental results demonstrating that Aβ_{42} remains well embedded in the lipid environment composed of POPC or POPC/SM/Chol [25]. The stable β structure seen in our simulations is also in agreement with experimental work, finding that Aβ_{40} is present as a β-sheet in a POPC bilayer [28]. Also, for Aβ_{42}, the β state in the membrane hydrophobic core of a POPC/POPS mixed bilayer could be identified to be destabilizing the membrane by increasing its permeability [27]. The formation of β-sheet between two peptides was also reported in a recent simulation study probing the self-assembly of Aβ in a mixed DPPC/cholesterol bilayer [59]. We observed the highest transmembrane stability for the β-sheet tetramer, which is supported by experimental work reporting that Aβ_{42} forms stable tetramers within membranes [29].

The simulations with DPPC resulted in a more pronounced loss of secondary structure for both SHEET and HEL-16 conformations within the membrane core as compared to the corresponding POPC and POPG simulations. In addition to a larger hydrophobic mismatch, the higher simulation temperature in the MD simulations with DPPC may also add to more fluctuations in the peptide. The HEL-23 conformation, however, adopts a stable α-helix inside the membrane. Our findings for the helical structures inserted in a DPPC bilayer are different than those obtained from MD simulations by Xu et al. [54]. They inserted the helical structure with K28 at the DPPC membrane–water interface and observed that Aβ_{40} left the hydrophobic core in less than 100 ns associating with the bilayer surface, where it remained α-helical. These discrepancies may be due to any or all of the following: (i) the missing two hydrophobic residues I41 and A42 in Aβ_{40}, (ii) the different initial insertion depths, (iii) usage of different force fields, and (iv) different protocols employed to insert the peptide into the membrane [48]. Other MD simulations with Aβ_{40} in a DPPC bilayer reported that the peptide remained partially embedded in the bilayer when it was inserted with K28 at the membrane–water interface [48]. Moreover, a complete loss of helicity was observed within the first 10 ns of these simulations. When Aβ_{40} was inserted with K16 at the interface, the peptide remained embedded in the bilayer and retained its α-helicity in the central segment [48], which is in agreement with our results.

The variety of simulation results points to the possibility that none of the MD simulations performed so far [48,54] fully describes the equilibrium configurational distribution of the peptides and membranes. This conclusion also includes our simulations, even though our simulations were performed on a 500 ns time scale. On much longer timescales—probably beyond microsecond timescales—major configurational changes and membrane translocation of Aβ could take place. Studying these processes is prohibitively expensive using

all-atom MD simulations, requiring coarse-grained and/or advanced sampling techniques instead.

3.8. Water permeation

Strong interactions between the Aβ_{42} peptide and lipids give rise to both disordering of the lipid headgroup arrangement and tilt of the lipids around the peptide. This tilt allows entry of water molecules into the hydrophobic membrane core, where they can form H-bonds with polar and non-polar Aβ_{42} residues. Some of these water molecules manage to cross to the other side of the lipid bilayers. Here, we observe the largest number of translocation events in the DPPC simulations (see Table 1). Among the POPC and POPG simulations we find the largest membrane permeability for the β-sheet tetramer in POPC, which is, however, not increased compared to the peptide-free bilayers. In the 100 ns MD runs of peptide-free lipid bilayers, we observed one permeating H_2O molecule for both POPC and POPG, while four water molecules translocated through the DPPC bilayer. It thus follows that the investigated Aβ_{42} structures do not increase the water translocation compared with the lipid-only bilayers; in some cases the presence of transmembrane Aβ_{42} even diminishes this process. There was no penetration and translocation of ions in any of the simulated systems.

In order to understand the different water permeabilities in the different bilayers, we have to consider the diffusion of water across the membranes and the interactions between transmembrane H_2O molecules and Aβ_{42}. In general, water molecules cross lipid membranes by two pathways, which one calls the lipid pathway and the water channel pathway. The lipid pathway refers to water crossing the lipid bilayer by diffusion while the water channel pathway results from membrane proteins, which provide an aqueous channel through which water can pass. In the latter case the water flux is very high and cannot be accounted for by water diffusion across lipid barriers. The water permeability for the lipid pathway can be approximated by a 3-slab model, where the inverse of the permeability P is equal to the sum of the two headgroup resistances and the hydrocarbon resistance [84]:

$$\frac{1}{P} = \frac{2}{P_h} + \frac{1}{P_c} \, . \tag{2}$$

Here, P_h is the permeability through the headgroup region and P_c is the permeability through the hydrocarbon core. For simplicity, P_c is assumed to have the form for a homogeneous hydrocarbon slab of thickness Δ_c [84]:

$$P_c = \frac{KD_c}{\Delta_c} \, , \tag{3}$$

where K is the partition coefficient of water into the hydrocarbon slab and D_c is the coefficient of diffusion of water within the hydrocarbon region. The 3-slab model assumes that the headgroups act as a partial barrier for entry of water into the hydrocarbon region. To account for the fractional area that is open to the entry of water molecules, a structural factor given by $(A - A_0)/A$ is used, where A_0 is the headgroup barrier area at which the permeability approximates to zero. Then, the theory states: [84]

$$P_h = \left(\frac{KD_h}{\Delta_h}\right)\left(\frac{A - A_0}{A}\right), \tag{4}$$

where K is again the same partition coefficient, D_h is the effective coefficient of diffusion in the headgroup region and Δ_h is its thickness. Eq. (4) shows that the permeability increases with increasing area per lipid, which corresponds to decreasing lipid chain order.

Since the headgroups are identical for POPC and DPPC, Δ_h and A_0 are the same for both lipids. However, the water diffusion depends on the actual temperature, thus D_h will be different in the DPPC and POPC simulations. In order for the theory to predict a larger P for DPPC at 325 K than for POPC at 298 K, Eqs. (2) to (4) require (i) a larger K and/or (ii) larger D_h and D_c to compensate for the effects of the larger thickness Δ_c and smaller A of DPPC. Measurements by Schatzberg showed that for n-hexadecane the water solubility increases 2.3-fold by increasing the temperature from 298 K to 318 K [85]. At 325 K we expect the increase of K to be even more pronounced. Turning to the effect of water diffusion in the hydrocarbon chain region, measurements of the diffusion of water through hydrocarbon liquids showed that D_c increases by a factor of 1.44 in n-hexadecane when the temperature is increased from 298 K to 318 K [85]. For the self-diffusion of water in water, denoted D_w, the following temperature dependence was found [86]:

$$D_w(T) = D_w(298) + 0.06 \times 10^{-9} \mathrm{m^2\ s^{-1}\ K^{-1}} (T - 298) \, , \tag{5}$$

with the diffusion of water in water at 298 K being $D_w(298) = 4.3 \times 10^{-9} \mathrm{m^2\ s^{-1}}$ for the SPC water model [87]. It follows that $D_w(325)$ is $5.92 \times 10^{-9} \mathrm{m^2\ s^{-1}}$, which is about 1.38 times higher than $D_w(298)$. One can thus assume that the rate of water diffusion in the headgroup regions is also about a 1.4 times higher at 325 K compared to 298 K.

The increased water permeation seen in our DPPC simulations is therefore a composite effect of increased water diffusion resulting from the increased simulation temperature of 325 K, and the larger partition coefficient of water in DPPC compared to POPC near the headgroup regions resulting from the reduced lipid order in the vicinity of Aβ_{42}. To test this conclusion we performed a 100 ns simulation of SHEET in POPC at 325 K. In this short time 14 H_2O molecules were able to pass the membrane. To a large degree this markedly increased water permeability is due to an increased water partition coefficient K for POPC at 325 K, as this temperature is well above the transition from the gel to liquid phase for this lipid type. It has been shown that the permeability of (poly)unsaturated PC lipids rises exponentially with increase in reduced temperature $(T - T_m)/T_m$, where T_m is the gel-to-liquid crystalline phase transition temperature [88].

The above reasoning allows explaining the increased membrane permeation of DPPC compared to POPC and POPG bilayers. However, the water translocation in our simulations is further complicated by interactions of the water molecules entering the lipid bilayers with the inserted Aβ_{42} peptide. To illustrate this process, snapshots of a water molecule crossing the POPC bilayer at 298 K in the vicinity of the SHEET structure are shown in Fig. 6. The whole translocation process takes about 12 ns. Most of the time the water molecule spends in the hydrophobic core interacting, via H-bond formation, either with the polar residue G31 or with residue V40, which is close to the polar residues G37 and G38, and the negatively charged C-terminus. These interactions induce a decelerated translocation process compared to the peptide-free bilayers, where the membrane passage of water is generally faster; in some cases it is even by a factor of twenty faster. A more detailed analysis of the translocation times can be found in the Supporting material.

It should finally be noted that the above discussion of water permeation is based on the use of non-polarizable force fields, which leads to an increase of ≈ 1 kcal mol^{-1} of the free-energy barrier for transfer of a water molecule from bulk to the interior of a 1,2-dimyristoyl-sn-glycero-3-phosphatidylcholine (DMPC) bilayer compared to when polarizable models for DMPC and water are employed [89]. The reduced free-energy barrier computed with the latter force field (4.5–5.5 kcal mol^{-1}) results from the decrease of the average water dipole moment from 2.6 D in bulk to 1.88 D in membrane interior, which is, compared to experiment, correctly predicted by the polarizable water model. However, since non-polarizable force fields were used in all our simulations, the findings of our water permeation analysis should not be affected.

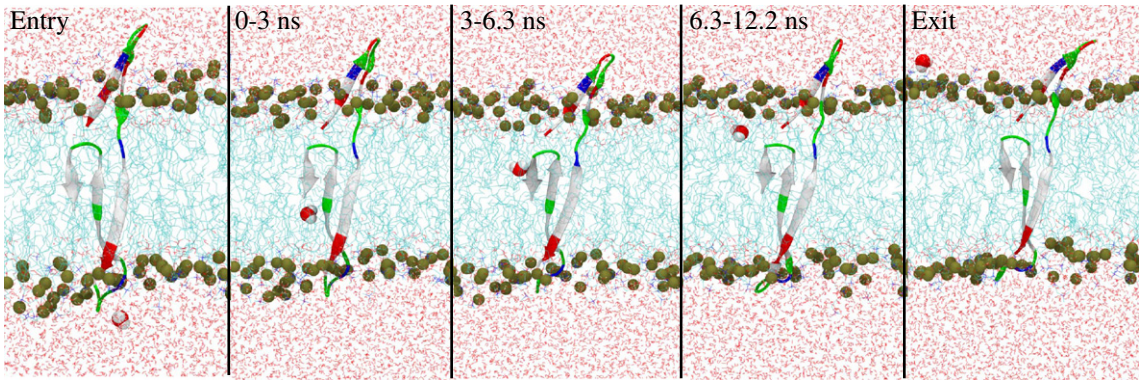

Fig. 6. Five snapshots depicting the process of water permeating through a POPC bilayer with an inserted Aβ_{42} peptide in the SHEET structure.

4. Conclusions

Association of Aβ with neuronal cell membranes and resulting neuronal toxicity is a well known AD hypothesis [90] with Aβ exerting its cytotoxic effect by increasing membrane fluidity [24]. Previously, it was reported that permeabilization of membranes was caused by Aβ oligomers [26], but later it was shown that the Aβ_{42} monomer can also intercalate the membrane and alter its properties [25]. There is increasing evidence that Aβ adopts a β conformation in the membrane [27,28], yet an experimental atomistic model of membrane-bound Aβ is still lacking. Molecular simulations offer the potential of predicting such structures [46,83,91], and, in addition, provide information about conformational transitions of Aβ and it interactions with lipid bilayers. To this end, we performed molecular simulations of transmembrane Aβ_{42} considering both helical and β-sheet conformations preinserted in POPC, DPPC and POPG bilayers. The MD simulations on the sub-microsecond timescale revealed the highest stability in POPC for both helical and β-sheet Aβ_{42}. Hydrophobic mismatch and lipid order of DPPC, and anionic surface charges of POPG bilayers are responsible for structural instabilities of Aβ_{42} in these bilayers. However, Aβ_{42} remained embedded in the bilayers in all of our MD simulations. The stability of the transmembrane β-sheet structure can be increased via oligomerization, where favorable interpeptide interactions, especially the formation of interpeptide H-bonds add to the stability of this structure [46].

We observed the translocation of one or more water molecules in the vicinity of the membrane-inserted Aβ_{42}. An in-depth analysis of this process revealed that Aβ_{42}-mediated water permeation is generally fast (within a few nanoseconds) yet generally slower than in the peptide-free bilayers. It is governed by a number of factors:

1. The lipid type, as it influences the water permeation via the area per lipid and partition coefficient of water.
2. The simulation temperature, as it influences the diffusion of water and solubility of water in the membranes.
3. The Aβ_{42} structure, as the rate limiting step is the membrane permeation in the hydrophobic core due to interactions between Aβ_{42} and the penetrating H_2O molecules.

Compared to the monomeric Aβ_{42} structures in POPC, the β-sheet tetramer increases the translocation of water through the POPC bilayers. This finding allows us to conclude that membrane permeabilization by membrane-bound Aβ must be due to Aβ oligomers, which is in agreement with experimental findings [26].

Our simulation studies were performed with model lipid bilayers composed of only one or two lipid types. Studying the behavior of Aβ in a more complex, neuronal membrane mimicking model bilayer would certainly help the understanding of the pathogenicity underlying AD [50,58,59]. Furthermore, the length and time scales of the simulations need to be extended in order to study the Aβ membrane association and its effect on membrane maintenance. Experimental work focused on resolving the structure of Aβ in and on lipid membranes would assist in modeling the molecular events leading to AD.

Acknowledgements

CP and BS gratefully acknowledge the Jülich Supercomputing Centre for providing and maintaining the computing resources used in this work (Computing time grant JISB32). Work at the University of Hertfordshire made use of the Science and Technology Research Institute high-performance computing facility. We thank Kenneth L. Osborne for proofreading the manuscript.

Appendix A. Supplementary data

Supplementary data to this article can be found online at http://dx.doi.org/10.1016/j.bbamem.2012.09.001.

References

[1] D.J. Selkoe, The origins of Alzheimer disease — a is for amyloid, J. Am. Med. Assoc. 283 (2000) 1615–1617.
[2] E.D. Roberson, L. Mucke, 100 years and counting: prospects for defeating Alzheimer's disease, Science 314 (2006) 781–784.
[3] G. Thinakaran, E.H. Koo, Amyloid precursor protein trafficking, processing, and function, J. Biol. Chem. 283 (2008) 29615–29619.
[4] J.T. Jarrett, E.P. Berger, P.T. Lansbury, The carboxy terminus of the beta-amyloid protein is critical for the seeding of amyloid formation - implications for the pathogenesis of Alzheimers-disease, Biochemistry 32 (1993) 4693–4697.
[5] S.G. Younkin, The role of A beta 42 in Alzheimer's disease, J. Physiol. Paris 92 (1998) 289–292.
[6] A. Mohamed, E.P. de Chaves, A internalization by neurons and glia, Int. J. Alzheimers Dis. 2011 (2011) 127984.
[7] T.L. Williams, L.C. Serpell, Membrane and surface interactions of Alzheimers Aβ peptide — insights into the mechanism of cytotoxicity, FEBS J. 278 (2011) 17.
[8] S.M. Butterfield, H.A. Lashuel, Amyloidogenic protein-membrane interactions: mechanistic insight from model systems, Angew. Chem. Int. Ed. Engl. 49 (2010) 5628–5654.
[9] E. Terzi, G. Holzemann, J. Seelig, Interaction of Alzheimer beta-amyloid peptide(1–40) with lipid membranes, Biochemistry 36 (1997) 14845–14852.
[10] A. Buchsteiner, T. Hauss, S. Dante, N.A. Dencher, Alzheimer's disease amyloid-beta peptide analogue alters the ps-dynamics of phospholipid membranes, Biochim. Biophys. Acta 1798 (2010) 1969–1976.
[11] G.P. Eckert, W.G. Wood, W.E. Mueller, Lipid membranes and beta-amyloid: a harmful connection, Curr. Protein Pept. Sci. 11 (2010) 319–325.
[12] F.J. Sepulveda, J. Parodi, R.W. Peoples, C. Opazo, L.G. Aguayo, Synaptotoxicity of Alzheimer beta amyloid can be explained by its membrane perforating property, PLoS One 5 (2010).
[13] M.P. Mattson, B. Cheng, D. Davis, K. Bryant, I. Lieberburg, R.E. Rydel, Beta-amyloid peptides destabilize calicum homeostasis and render human cortical-neurons vulnerable to excitotoxicity, J. Neurosci. 12 (1992) 376–389.
[14] I. Peters, U. Igbavboa, T. Schuett, S. Haidari, U. Hartig, X. Rosello, S. Boettner, E. Copanaki, T. Deller, D. Koegel, W.G. Wood, W.E. Mueller, G.P. Eckert, The interaction of beta-amyloid protein with cellular membranes stimulates its own production, Biochim. Biophys. Acta 1788 (2009) 964–972.
[15] E. Terzi, G. Hölzemann, J. Seelig, Interaction of Alzheimer-amyloid peptide(1–40) with lipid membranes, Biochemistry 36 (1997) 14845–14852.
[16] C. Ege, K. Lee, Insertion of Alzheimer's abeta 40 peptide into lipid monolayers, Biophys. J. 87 (2004) 1732–1740.

[17] E. Terzi, G. Holzemann, J. Seelig, Alzheimer beta-amyloid peptide 25–35: electrostatic interactions with phospholipid membranes, Biochemistry 33 (1994) 7434–7441.
[18] J. McLaurin, A. Chakrabartty, Characterization of the interactions of Alzheimer β-amyloid peptides with phospholipid membranes, Eur. J. Biochem. 245 (1997) 355–363.
[19] C. Ege, J. Majewski, G. Wu, K. Kjaer, K. Lee, Templating effect of lipid membranes on Alzheimer's amyloid beta peptide, Chemphyschem 6 (2005) 226–229.
[20] A. Chauhan, I. Ray, V. Chauhan, Interaction of amyloid beta-protein with anionic phospholipids: possible involvement of lys28 and c-terminus aliphatic amino acids, Neurochem. Res. 25 (2000) 423–429.
[21] E.Y. Chi, C. Ege, A. Winans, J. Majewski, G. Wu, K. Kjaer, K.Y.C. Lee, Lipid membrane templates the ordering and induces the fibrillogenesis of Alzheimer's disease amyloid-peptide, Proteins 72 (2008) 1–24.
[22] M. Coles, W. Bicknell, A.A. Watson, D.P. Fairlie, D.J. Craik, Solution structure of amyloid beta-peptide(1–40) in a water-micelle environment. Is the membrane-spanning domain where we think it is? Biochemistry 37 (1998) 11064–11077.
[23] E. Tischer, B. Cordell, Beta-amyloid precursor protein — location of transmembrane domain and specificity of gamma-secretase cleavage, J. Biol. Chem. 271 (1996) 21914–21919.
[24] R.P. Mason, R.F. Jacob, M.F. Walter, P.E. Mason, N.A. Avdulov, S.V. Chochina, U. Igbavboa, W.G. Wood, Distribution and fluidizing action of soluble and aggregated amyloid beta-peptide in rat synaptic plasma membranes, J. Biol. Chem. 274 (1999) 18801–18807.
[25] E.E. Ambroggio, D.H. Kim, F. Separovic, C.J. Barrow, K.J. Barnham, L.A. Bagatolli, G.D. Fidelio, Surface behavior and lipid interaction of Alzheimer beta-amyloid peptide 1–42: a membrane-disrupting peptide, Biophys. J. 88 (2005) 2706–2713.
[26] R. Kayed, Y. Sokolov, B. Edmonds, T.M. McIntire, S.C. Milton, J.E. Hall, C.G. Glabe, Permeabilization of lipid bilayers is a common conformation-dependent activity of soluble amyloid oligomers in protein misfolding diseases, J. Biol. Chem. 279 (2004) 46363–46366.
[27] T.L. Lau, E.E. Ambroggio, D.J. Tew, R. Cappai, C.L. Masters, G.D. Fidelio, K.J. Barnham, F. Separovic, Amyloid-beta peptide disruption of lipid membranes and the effect of metal ions, J. Mol. Biol. 356 (2006) 759–770.
[28] M.R.R. de Planque, V. Raussens, S.A. Contera, D.T.S. Rijkers, R.M.J. Liskamp, J.M. Ruysschaert, J.F. Ryan, F. Separovic, A. Watts, β-sheet structured beta-amyloid(1–40) perturbs phosphatidylcholine model membranes, J. Mol. Biol. 368 (2007) 982–997.
[29] H. Lin, R. Bhatia, R. Lal, Amyloid β protein forms ion channels: implications for Alzheimer's disease pathophysiology, FASEB J. 15 (2001) 2433–2444.
[30] A. Quist, I. Doudevski, H. Lin, R. Azimova, D. Ng, B. Frangione, B. Kagan, J. Ghiso, R. Lal, Amyloid ion channels: a common structural link for protein misfolding disease, Proc. Natl. Acad. Sci. U. S. A. 102 (2005) 10427–10432.
[31] N. Arispe, H. Pollard, E. Rojas, β-amyloid Ca^{2+}-channel hypothesis for neuronal death in Alzheimer disease, Mol. Cell. Biochem. 140 (1994) 119–125.
[32] H. Lin, Y. Zhu, R. Lal, Amyloid β protein (1–40) forms calcium-permeable, Zn^{2+}-sensitive channel in reconstituted lipid vesicles, Biochemistry 38 (1999) 11189–11196.
[33] S.K. Rhee, A.P. Quist, R. Lal, Amyloid β protein-(1–42) forms calcium-permeable, Zn^{2+}-sensitive channel, J. Biol. Chem. 273 (1998) 13379–13382.
[34] Y. Hirakura, M.C. Lin, B.L. Kagan, Alzheimer amyloid AB_{1-42} channels: effects of solvent, pH, and congo red, J. Neurosci. Res. 57 (1999) 458–466.
[35] R. Friedman, Aggregation of amyloids in a cellular context: modelling and experiment, Biochem. J. 438 (2011) 415–426.
[36] J.E. Straub, D. Thirumalai, Toward a molecular theory of early and late events in monomer to amyloid fibril formation, Annu. Rev. Phys. Chem. 62 (2011) 437–463.
[37] H. Jang, J. Zheng, R. Lal, R. Nussinov, New structures help the modeling of toxic amyloid beta ion channels, Trends Biochem. Sci. 33 (2008) 91–100.
[38] H. Jang, J. Zheng, R. Nussinov, Models of beta-amyloid ion channels in the membrane suggest that channel formation in the bilayer is a dynamic process, Biophys. J. 93 (2007) 1938–1949.
[39] H. Jang, F.T. Arce, R. Capone, S. Ramachandran, R. Lal, R. Nussinov, Misfolded amyloid ion channels present mobile beta-sheet subunits in contrast to conventional ion channels, Biophys. J. 97 (2009) 3029–3037.
[40] H. Jang, F. Arce, M. Mustata, S. Ramachandran, R. Capone, R. Nussinov, R. Lal, Antimicrobial protegrin-1 forms amyloid-like fibrils with rapid kinetics suggesting a functional link, Biophys. J. 100 (2011) 1775–1783.
[41] R. Capone, M. Mustata, H. Jang, F.T. Arce, R. Nussinov, R. Lal, Antimicrobial protegrin-1 forms ion channels: molecular dynamic simulation, atomic force microscopy, and electrical conductance studies, Biophys. J. 98 (2010) 2644–2652.
[42] R. Capone, H. Jang, S.A. Kotler, B.L. Kagan, R. Nussinov, R. Lal, Probing structural features of Alzheimer's amyloid-beta pores in bilayers using site-specific amino acid substitutions, Biochemistry 51 (2012) 776–785.
[43] F.T. Arce, H. Jang, S. Ramachandran, P.B. Landon, R. Nussinov, R. Lal, Polymorphism of amyloid beta peptide in different environments: implications for membrane insertion and pore formation, Soft Matter 7 (2011) 5267–5273.
[44] R. Capone, H. Jang, S.A. Kotler, L. Connelly, F.T. Arce, S. Ramachandran, B.L. Kagan, R. Nussinov, R. Lal, All-d-enantiomer of β-amyloid peptide forms ion channels in lipid bilayers, J. Chem. Theory Comput. 8 (2012) 1143–1152.
[45] L. Connelly, H. Jang, F.T. Arce, R. Capone, S.A. Kotler, S. Ramachandran, B.L. Kagan, R. Nussinov, R. Lal, Atomic force microscopy and MD simulations reveal pore-like structures of all-d-enantiomer of Alzheimer's β-amyloid peptide: relevance to the ion channel mechanism of ad pathology, J. Phys. Chem. B 116 (2012) 1728–1735.
[46] B. Strodel, J. Lee, C. Whittleston, D. Wales, Transmembrane structures for Alzheimer's $A\beta_{1-42}$ oligomers, J. Am. Chem. Soc. 132 (2010) 13300–13312.
[47] Z. Chang, Y. Luo, Y. Zhang, G. Wei, Interactions of $A\beta_{25-35}$ β-barrel-like oligomers with anionic lipid bilayers and resulting membrane leakage: an all-atom molecular dynamics study, J. Phys. Chem. B 115 (2011) 1165–1174.
[48] J.A. Lemkul, D.R. Bevan, A comparative molecular dynamics analysis of the amyloid beta-peptide in a lipid bilayer, Arch. Biochem. Biophys. 470 (2008) 54–63.
[49] J.A. Lemkul, D.R. Bevan, Perturbation of membranes by the amyloid beta-peptide — a molecular dynamics study, FEBS J. 276 (2009) 3060–3075.
[50] J.A. Lemkul, D.R. Bevan, Lipid composition influences the release of Alzheimer's amyloid beta-peptide from membranes, Protein Sci. 20 (2011) 1530–1545.
[51] C.H. Davis, M.L. Berkowitz, Interaction between amyloid-beta peptide and phospholipid bilayers: a molecular dynamics study, Biophys. J. 96 (2009) 785–797.
[52] C.H. Davis, M.L. Berkowitz, Structure of the amyloid-beta (1–42) monomer absorbed to model phospholipid bilayers: a molecular dynamics study, J. Phys. Chem. B 113 (2009) 14480–14486.
[53] C.H. Davis, M.L. Berkowitz, A molecular dynamics study of the early stages of amyloid-beta(1–42) oligomerization: the role of lipid membranes, Proteins 78 (2010) 2533–2545.
[54] Y.C. Xu, J.J. Shen, X.M. Luo, W.L. Zhu, K.X. Chen, J.P. Ma, H.L. Jiang, Conformational transition of amyloid beta-peptide, Proc. Natl. Acad. Sci. U. S. A. 102 (2005) 5403–5407.
[55] N. Miyashita, J.E. Straub, D. Thirumalai, Structures of β-amyloid peptide 1–40, 1–42, and 1–55—the 672–726 fragment of APP-in a membrane environment with implications for interactions with γ-secretase, J. Am. Chem. Soc. 131 (2009) 17843–17852.
[56] R. Friedman, R. Pellarin, A. Caflisch, Amyloid aggregation on lipid bilayers and its impact on membrane permeability, J. Mol. Biol. 387 (2009) 407–415.
[57] R. Friedman, R. Pellarin, A. Caflisch, Soluble protofibrils as metastable intermediates in simulations of amyloid fibril degradation induced by lipid vesicles, J. Phys. Chem. Lett. 1 (2010) 471–474.
[58] J. Zhao, Q. Wang, G. Liang, J. Zheng, Molecular dynamics simulations of low-ordered Alzheimer beta-amyloid oligomers from dimer to hexamer on self-assembled monolayers, Langmuir 27 (2011) 14876–14887.
[59] L.N. Zhao, S.W. Chiu, J. Benoit, L.Y. Chew, Y. Mu, Amyloid beta peptides aggregation in a mixed membrane bilayer: a molecular dynamics study, J. Phys. Chem. B 115 (2011) 12247–12256.
[60] C.J. Barrow, A. Yasuda, P.T. Kenny, M.G. Zagorski, Solution conformations and aggregational properties of synthetic amyloid β-peptides of Alzheimer's disease: Analysis of circular dichroism spectra, J. Mol. Biol. 225 (1992) 1075–1093.
[61] J.P. Lee, E.R. Stimson, J.R. Ghilardi, P.W. Mantyh, Y.A. Lu, A.M. Felix, W. Llanos, A. Behbin, M. Cummings, ^{1}H NMR of Aβ amyloid peptide congeners in water solution. Conformational changes correlate with plaque competence, Biochemistry 34 (1995) 5191–5200.
[62] T. Lührs, C. Ritter, M. Adrian, D. Riek-Loher, B. Bohrmann, H. Döbeli, D. Schubert, R. Riek, 3d structure of Alzheimer's amyloid-β(142) fibrils, Proc. Natl. Acad. Sci. U. S. A. 102 (2005) 17342–17347.
[63] A.T. Petkova, W.M. Yau, R. Tycko, Experimental constraints on quaternary structure in Alzheimer's β-amyloid fibrils, Biochemistry 45 (2006) 498–512.
[64] F. Massi, J.W. Peng, J.P. Lee, J.E. Straub, Simulation study of the structure and dynamics of the Alzheimer's amyloid peptide congener in solution, Biophys. J. 80 (2001) 31–44.
[65] J.E. Straub, J. Guevara, S. Huo, J.P. Lee, Long time dynamic simulations: exploring the folding pathways of an Alzheimer's amyloid Aβ-peptide, Acc. Chem. Res. 35 (2002) 473481.
[66] B. Ma, R. Nussinov, Stabilities and conformations of Alzheimer's β-amyloid peptide oligomers (Aβ(16–22), Aβ(16–35) and Aβ(10–35)): sequence effects, Proc. Natl. Acad. Sci. U. S. A. 99 (2002) 14126–14131.
[67] D.L. Mobley, D.L. Cox, R.R.P. Singh, M.W. Maddox, M.L. Longo, Modeling amyloid beta-peptide insertion into lipid bilayers, Biophys. J. 86 (2004) 3585–3597.
[68] J.L. MacCallum, W.F.D. Bennetta, D.P. Tieleman, Distribution of amino acids in a lipid bilayer from computer simulations, Biophys. J. 94 (2008) 3393–3404.
[69] S. Donnini, F. Tegeler, G. Groenhof, H. Grubmüller, Constant pH molecular dynamics in explicit solvent with λ-dynamics, J. Chem. Theory Comput. 7 (2011) 1962–1978.
[70] B. Hess, C. Kutzner, D. van der Spoel, E. Lindahl, Gromacs 4: algorithms for highly efficient, load-balanced, and scalable molecular simulation, J. Chem. Theory Comput. 4 (2008) 435–447.
[71] C. Oostenbrink, A. Villa, A.E. Mark, W.F.V. Gunsteren, A biomolecular force field based on the free enthalpy of hydration and solvation: the GROMOS force-field parameter sets 53A5 and 53A6, J. Comput. Chem. 25 (2004) 1656–1676.
[72] A. Kukol, Lipid models for united-atom molecular dynamics simulations of proteins, J. Chem. Theory Comput. 5 (2009) 615–626.
[73] O.O. Olubiyi, B. Strodel, Structures of the amyloid β-peptides $A\beta_{1-40}$ and $A\beta_{1-42}$ as influenced by pH and a D-peptide, J. Phys. Chem. B 116 (2012) 3280–3291.
[74] C. Kandt, W.L. Ash, D.P. Tieleman, Setting up and running molecular dynamics simulations of membrane proteins, Methods 41 (2007) 475–488.
[75] W. Kabsch, C. Sander, Dictionary of protein secondary structure — pattern-recognition of hydrogen-bonded and geometrical features, Biopolymers 22 (1983) 2577–2637.
[76] W. Humphrey, A. Dalke, K. Schulten, VMD — visual molecular dynamics, J. Mol. Graphics 14 (1996) 33–38.
[77] W.J. Allen, J.A. Lemkul, D.R. Bevan, GridMAT-MD: a grid-based membrane analysis tool for use with molecular dynamics, J. Comput. Chem. 30 (2009) 1952–1958.
[78] A. Cordomí, J.J. Perez, Molecular dynamics simulations of rhodopsin in different one-component lipid bilayers, J. Phys. Chem. B 111 (2007) 7052–7063.
[79] H.J. Kaiser, A. Orłowski, T. Róg, T.K.M. Nyholm, W. Chai, T. Feizi, D. Lingwood, I. Vattulainen, K. Simons, Lateral sorting in model membranes by cholesterol-mediated hydrophobic matching, Proc. Natl. Acad. Sci. U. S. A. 108 (2011) 16628–16633.
[80] A.A. Gurtovenko, I. Vattulainen, Calculation of the electrostatic potential of lipid bilayers from molecular dynamics simulations: methodological issues, J. Chem. Phys. 130 (2009) 215107.
[81] A.A. Gurtovenko, I. Vattulainen, Intrinsic potential of cell membranes: opposite effects of lipid transmembrane asymmetry and asymmetric salt ion distribution, J. Phys. Chem. B 113 (2009) 7194–7198.

[82] S. McLaughlin, The electrostatic properties of membranes, Annu. Rev. Biophys. Biophys. Chem. 18 (1989) 113–136.
[83] Y. Shafrir, S. Durell, N. Arispe, H.R. Guy, Models of membrane-bound Alzheimer's Abeta peptide assemblies, Proteins 78 (2010) 3473–3487.
[84] S. Tristram-Nagle, D. Kim, N. Akhunzada, N. Kučerka, J.C. Mathai, J. Katsaras, M. Zeidel, J. Nagle, Structure and permeability of fully hydrated diphytanoylPC, Chem. Phys. Lipids 163 (2010) 630–637.
[85] P. Schatzberg, Diffusion of water through hydrocarbon liquids, J. Polym. Sci. Part C: Polym. Lett. 10 (1965) 87–92.
[86] R. Mills, Self-diffusion in normal and heavy water in the range 1–45 °C, J. Phys. Chem. 77 (1973) 685–688.
[87] P. Mark, L. Nilsson, Structure and dynamics of the TIP3P, SPC, and SPC/E water models at 298 K, J. Phys. Chem. A 105 (2001) 9954–9960.
[88] K. Olbrich, W. Rawicz, D. Needham, E. Evans, Water permeability and mechanical strength of polyunsaturated lipid bilayers, Biophys. J. 79 (2000) 321–327.
[89] B.A. Bauer, T.R. Lucas, D.J. Meninger, S. Patel, Water permeation through dmpc lipid bilayers using polarizable charge equilibration force fields, Chem. Phys. Lett. 508 (2011) 289–294.
[90] O. Wirths, G. Multhaup, T.A. Bayer, A modified beta-amyloid hypothesis: intraneuronal accumulation of the beta-amyloid peptide—the first step of a fatal cascade, J. Neurochem. 91 (2004) 513–520.
[91] S. Durell, H. Guy, N. Arsipe, E. Rojas, H. Pollard, Theoretical models of the ion channel structure of amyloid β-protein, Biophys. J. 67 (1994) 2137–2145.
[92] N. Kučerka, S.T. Nagle, J.F. Nagle, Structure of fully hydrated fluid phase lipid bilayers with monounsaturated chains, J. Membr. Biol. 208 (2005) 193–202.
[93] N. Kučerka, S.T. Nagle, J.F. Nagle, Closer look at structure of fully hydrated fluid phase DPPC bilayers, Biophys. J. 90 (2006) L83–L85.
[94] N. Kučerka, B.W. Holland, C.G. Gray, B. Tomberli, J. Katsaras, Scattering density profile model of POPG bilayers as determined by molecular dynamics simulations and small-angle neutron and X-ray scattering experiments, J. Phys. Chem. B 116 (2012) 232–239.